**JOURNAL OF HIGH-FREQUENCY COMMUNICATION TECHNOLOGIES**
*Vol. 01 (01) (2023), pp.43-54*
https://doi.org/10.58399/WXEJ1376

# Electronically Controlled Frequency Agile Beam Scanning Reflectarray Antenna with Integrated Control Unit

**Kavitha Narayanaswamy**[1*], **Kirubaveni Savarimuthu**[2], **Ikram Khan**[3]

[1,2] Department of ECE, Sri Sivasubramaniya Nadar College of Engineering, Kalavakkam, Chennai-603110, India *E-mail address: kavithan@ssn.edu.in, kirubavenis@ssn.edu.in,*
[3] ISMO Bio-Photonics Pvt Ltd technologies, IITM RP, Kanagam Road, Taramani, Chennai, India *E-mail address: ikram@ismobiophotonics.com*

**Abstract**

This paper reports the design, development, fabrication, and testing of a 225-element reconfigurable reflectarray (RRA) antenna with frequency agility and beam steering capabilities. The 15 × 15 (18.75 cm) RRA operating in the Ku-band downlink frequency range (11.8 -12.2 GHz) of fixed satellite services (FSS) produces dual resonances switched between uplink frequency range (15-18 GHz) of FSS and earth exploration satellite range of 9.5-9.8 GHz (X-band). To attain reconfigurable multiple resonances, the unit cell is designed with a Malta cross of varying slot lengths interconnected to a square ring via a PIN diode. In the OFF state of the PIN diode connected between the concentric elements, a phase variation of 360 ° is obtained at 12 GHz and 9.5 GHz by varying the size of the Malta cross. By increasing the width of the outer ring in the ON state of the PIN diode, a dual resonance is obtained at 12 GHz and 17 GHz with 360° phase agility. The beam scanning is attempted at X-band frequency by controlling the capacitance offered by the varactor diode connected between an inductive element and Malta cross. The proposed RRA offers 22.16 dBi, 24.5 dBi, and 18.43 dBi simulated gain at 17 GHz, 12 GHz, and 9.5 GHz, respectively. The simulated sidelobe levels (SLLs) and cross-polarization levels are -14.7 dB and less than -32 dB, respectively. The proposed compound reconfigurable reflectarray befits fixed and mobile satellites, earth exploration satellites, radiolocation, aeronautical radio navigation, and deep space research.

***Keywords***: *Reflectarray; Reconfigurable; FSS; Frequency agility;Beam Scanning; PIN diode; Varactor diode; DAC control board*

## 1. Introduction

Emergency circumstances confronted in radar applications, deep space, and satellite communication more often are coupled with several complications. A solution to such intricate conditions requires easily deployable reconfigurable antennas that satiate the need for high gain, high efficiency, high reliability, fast scanning, and low-loss control circuitry (Montori et al., 2015). Compound reconfigurable reflectarray (RRA) antennas, in addition to beamforming, afford beam switching and wide-angle beam scanning by controlling the phase compensation of individual array elements

*Corresponding author
Received: 03$^{rd}$, December 2022, Revised: 19$^{th}$ January, 2023 Accepted: 02$^{nd}$ March 2023 and available online 16$^{th}$ March 2023

This work is licensed under a Creative Commons Attribution 4.0 License(CC BY 4.0).
For more information, see https://creativecommons.org/licenses/by/4.0/

(Hum and Perruisseau-Carrier, 2014). The attributes, such as operating frequency, radiation pattern, and polarization of RA can be reconfigured to befit targeted application (Costanzo et al., 2018). Many researchers (Costanzo et al., 2018),(Li et al., 2021), (Rodrigo et al., 2013a), (Rodrigo et al., 2013b), (Ismail et al., 2010), (Gu et al., 2017), (Hajian), (Han et al., 2019), (Zhang et al., 2019), (Li and Abbosh, 2015), (Yang et al., 2016), (Carrasco et al., 2012), (Yang et al., 2017), (Xu et al., 2020), (Venneri et al., 2013), (Narayanasamy et al., 2020), (Hum et al., 2007), (Boccia et al., 2010), (Tayebi et al., 2015) and (Trampler et al., 2020) have explored the reconfiguration ability of RAs for various applications using diverse mechanisms.

As frequency reconfigurable antennas exhibit high non-interference ability and high spectrum utilization (Li et al., 2021), researchers in (Costanzo et al., 2018),(Li et al., 2021), (Rodrigo et al., 2013a), (Rodrigo et al., 2013b), (Ismail et al., 2010) and (Gu et al., 2017) have reported various mechanisms to achieve frequency reconfiguration in reflectarrays. Researchers in (Rodrigo et al., 2013a) and (Rodrigo et al., 2013b) have obtained continuous frequency tuning from 1.88 GHz to 3.07 GHz with a 270° phase variation using four metal patches interconnected by radio frequency (RF) switches and a varactor diode. In (Ismail et al., 2010), a frequency reconfigurable unit cell operating at 10 GHz is presented. Frequency tuning from 9.9 to 8.1 GHz and 10.1 to 11.8 GHz are obtained by introducing different types of slots in the patches. Similarly, in (Li et al., 2021), the controlled activation of two RF micro-electromechanical system (MEMS) switches interconnecting three multi-scaled patches of a 16-element array produces beam switching at three different resonant frequencies in X (8.6 GHz), Ku (17.1 GHz), and Ka (31.1 GHz) bands. Hence, unlike phased arrays, reconfiguration in RAs is achieved without a complex and lossy feed network. Similarly, unlike the mechanical steering in parabolic reflectors, instantaneous positioning of the beam in the desired direction at high data rates is viable in RAs without mechanical errors using electronic beam scanning (Hum and Perruisseau-Carrier, 2014). As stated in (Hajian), evaluation of beam steering is associated with the scanning range and complexity of the control circuit. With reduced complexity in the control circuitry, (Han et al., 2019), (Zhang et al., 2019), (Li and Abbosh, 2015), (Yang et al., 2016), (Carrasco et al., 2012), (Yang et al., 2017) and (Xu et al., 2020) report reconfiguration in RA using PIN diodes, RF MEMS, and gathered elements. In (Zhang et al., 2019), the radiation is scanned from -30° to 60° with a peak measured gain of 19.2 dBi and 25% aperture efficiency at 11.5 GHz using 196-element RRA. The 1-bit phase compensation utilized to produce beam scanning is obtained by controlling the PIN diode connected between each patch and the ground. The required biasing circuit and the diode are placed at the reverse side of the reflecting layers to avoid scattering losses from the diode and solders. However, the reported RRA suffers from a high sidelobe level ($<$ -10 dB) and large half-power beamwidth (11.4°). A similar 244 element X-band multi-layered RRA designed using square patches and gathered elements (Carrasco et al., 2012) produces beam scanned to -5, 0, +5 degrees with 24.9 dBi measured gain. Although the usage of gathering elements has reduced the number of control devices and the associated biasing circuit, the performance of the multi-layered structure reduces due to misalignment and fabrication errors. The researchers in (Yang et al., 2017) have fabricated a 1600 element RRA producing ±60° scanned beam at 11.1 GHz and 14.3 GHz with a measured peak gain of 29.3 dBi and 30.8 dBi, respectively. The reconfiguration is achieved using properly biased PIN diodes in each element. Very low 1-dB gain bandwidths of 0.5 and 0.9 GHz are obtained at the two operating bands. Another dual-band RRA reported in (Xu et al., 2020) produces 22.3 and 22.5 dBi peak gain at 12.5 and 14.25 GHz, respectively, using 256 elements. With a 3 dB gain bandwidth of 11.6% and 11.9%, beam scanning from -15° to -60° is produced at the dual frequencies by varying the switching conditions of two PIN diodes integrated with each element. Besides being advantageous in transmitting and receiving orthogonally polarized signals, misalignment error occurs in multilayer arrangements.

When compared with other active devices utilized in RRAs, varactor diodes having merits, such as nominal cost, negligible power consumption, nanosecond speed, and less mounting complexity (Venneri et al., 2013) offer continual beam switching. Hence, the researchers in (Narayanasamy et al., 2020), (Hum et al., 2007), (Boccia et al., 2010), (Tayebi et al., 2015) and (Trampler et al., 2020) have varied the phase offered by varactor-loaded RA elements using simple voltage controls to obtain different beam scanning angles. In (Venneri et al., 2013), a varactor-loaded microstrip line aperture coupled to the patch provides 360° tunability by including the capacitive and inductive effects through suitable stubs. The 45 element RA designed to operate at 11.5 GHz produces a

±25° scanned beam with a peak gain of 9.3 dBi. Another similar 49 element RRA (Trampler et al., 2020) with dual resonant cross-ring structures provide 437° phase variation at 10.7 GHz. With a measured gain of 15.03 dBi and a 3 dB gain bandwidth of 7.81%, ± 50° beam scanning range is observed by biasing the varactor diodes incorporated in each element.

Pursuant to the requisites of the desired application, frequency reconfigurable reflectarrays producing dynamic radiation patterns cover a wide range of frequencies (Rodrigo et al., 2013a) with significant radiation performances. Hence, the proposed compound RRA is developed for covering the Ku-band downlink and uplink frequencies required for FSS and X-band frequencies (9.5-9.8 GHz) (Department of Telecommunications, 2018) needed in earth exploration satellites. To obtain multiple resonances, a novel unit cell is designed using a Malta cross-patch of varied slot lengths enclosed within a square ring. The frequency tuning between the desired ranges is realized using a single PIN diode interconnecting the concentric patch and ring. Beam steering between ±10° , ±20° and ±30° in both the states of the PIN diode is attempted using a single varactor diode connected between the inner patch and an inductive element. The controlled biasing required for both the diodes is supplied through an electronic control board (ECB) designed specifically for this purpose. The simulated results are validated experimentally in anechoic chamber by integrating the fabricated prototype of RRA with ECB.

The organization of the article is as follows: the design of the unit cell and its reflection characteristic analysis is described in Section 2. Section 3 elaborates the design, fabrication, integration, and measurement of the compound RRA and the ECB. The analysis of simulated and measured results of RRA is presented in Section 4. This section includes the performance comparison of the proposed antenna with other antennas discussed in literature.

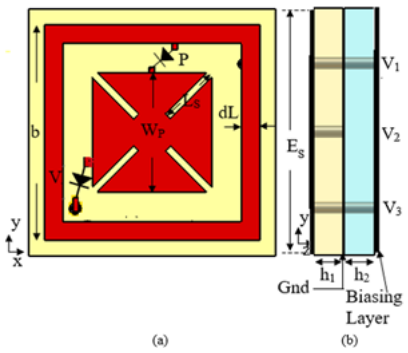


**Figure 1.** (a) Unit cell structure and (b) side view of the unit cell

## 2. Unit Cell Design and Characterization

With the objective of obtaining reconfigurable multiple resonances, a Malta cross-structure enclosed within a square ring is developed on a grounded 1.52-mm thick Taconic substrate. The Taconic TLY 5 is a low loss substrate whose relative permittivity is 2.2 and loss tangent $\tan\delta$ is 0.0009. The element size is maintained as 12.5 mm to ensure a periodicity of $0.39\lambda_0$, $0.5\lambda_0$, and $0.7\lambda_0$ at 9.5 GHz, 12 GHz, and 17 GHz, respectively. Frequency reconfiguration is attempted by switching ON and OFF a PIN diode interconnecting the outer ring and the Malta cross-patch. A varactor diode connecting an inductive element to the patch provides the phase shift required for steering the beam in desired directions. The biasing units of the diodes are etched on a 1.52-mm thick Rogers RO4003C substrate ($\varepsilon_r = 3.55$, $\tan\delta = 0.0027$). The biasing voltages required for the controlled operation of the diodes are supplied by the ECB through vias. Based on the user requirement, the DAC units in the ECB distribute the necessary biasing voltage to the diodes in each cell. Figure 1 depicts the structure of the unit cell with parameter indications and the layers of the unit cell with vias, $V_1$, $V_2$, $V_3$.

### 2.1. Evolution and parametric Analysis

The unit cell is modelled using infinite array approach as shown in Fig. 2(a) using CST microwave studio software. Initially, the unit cell design started with a square loop integrated to a delay line through a PIN diode. The designed unit cell is simulated in frequency domain under unit cell boundary conditions using plane wave excitation. The Floquet ports are set to observe the magnitude and phase of the reflection coefficient by varying the size of the Malta cross in PIN OFF condition. The structural changes offered only 260° phase variation without shift in resonant frequency during PIN ON condition. The delay line caused only an increase in the bandwidth of the resonance obtained. Hence, the concentric square rings are utilized with a PIN diode interconnecting them. Although dual resonance is obtained, the phase shift obtained is only 300°.

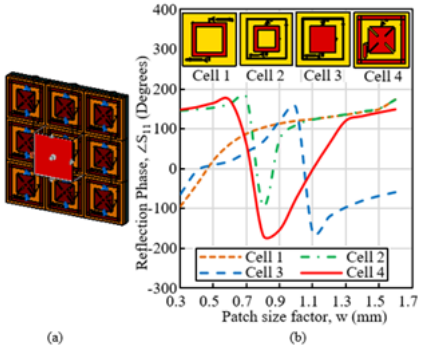


**Figure 2.** (a) Infinite array model of the proposed element and (b) unit cell evolution

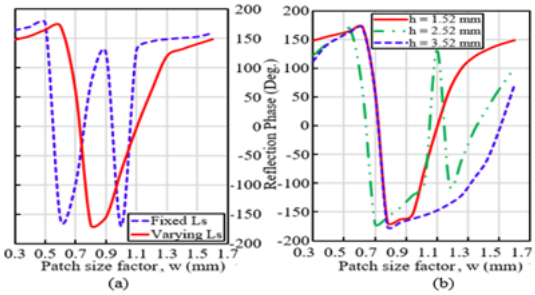


**Figure 3.** Reflection characteristics for (a) fixed and varied $L_s$ and (b) different substrate 1 thickness, $h_1$

Replacing the inner square ring by patch offered a phase variation of 320° with higher slope. Hence, to obtain 360° phase variation, the inner square patch is replaced by a Mata cross with diagonal slots of varying length. Thus, the proposed unit cell has a Malta cross enclosed within a square ring. Figure 2(b) depicts the unit cell evolution based on the phase characteristics of the element in the OFF state of the PIN diode. As resonances at three frequencies in two different bands closer to each other is set as objective, the degree of freedom in the structure is much limited. Hence, the parameters $L_s$, the length of Malta cross slot, and height of the Taconic substrate, $h_1$ are only optimized. The unit cell characteristics is simulated for a fixed and varied values of $L_s$. Figure 3(a) shows that for fixed value of $L_s$, the slope of the phase curve is very large when compared with the phase variation obtained for varying $L_s$ value. Hence, in the proposed design, the Malta cross slot length is varied in accordance with the change in Malta cross. As studied in the literatures, thicker substrates provide better bandwidth. Hence, the height of the Taconic substrate is increased to 2.52 mm and 3.52 mm and the characteristics is studied. It is evident from Fig. 3(b) that increase in the substrate height causes negligible difference in the unit cell performance. Hence to maintain low profile, a 1.52-mm thick substrate is preferred.

### 2.2. Element design and analysis

The optimized parameters of the proposed unit cell are presented in Table 1. One PIN diode interconnecting the outer ring and Malta cross is utilized in each element of the 225-element array to achieve frequency reconfiguration. As the reflection coefficient magnitude of the element

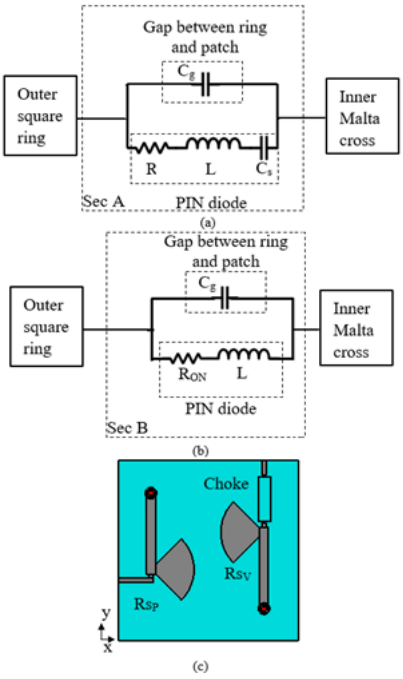


**Figure 4.** Switching operation of PIN diode (a) OFF state, (b) ON state, and (c) biasing circuit of the proposed unit cell

gets influenced by the series resistance of the diode, a diode of lower series resistance Skyworks SMP1340-079LF (Han et al., 2019) is chosen. For full wave simulation, the PIN diode in OFF state is modelled as series RLC circuit and in ON state, it acts as a series RL circuit. The parameter values in both states are presented in Table 2. These diodes are properly biased using a biasing circuit as depicted in Fig. 4(c). Owing to spatial feed, there is no direct connection between the DC source and the RF source. Hence, DC block capacitor is replaced by a quarter wavelength radial stub between the biasing lines and the diodes (Abbasi et al., 2020) to provide impedance matching. The biasing voltage required for the PIN diode's switching operation is provided through an SPDT switch connected between the external supply and the radial stub of the biasing circuit. During the OFF state of the PIN diode, the gap capacitance $C_g$ appears in shunt to the series RLC equivalent of the diode as shown in Fig. 4(a). The circuit (section 2.1) is similar to a crystal oscillator that produces a series and a parallel resonance at $f_1$ and $f_2$. The impedance of this section 2.1 is

$$Z_{OFF} = Z_{cg} \times Z_P / Z_{cg} + Z_P \tag{1}$$

where, $Z_{cg} = -jX_{cg}, Z_P = R + jX_L - jX_{cs} = R + j(X_L - X_{cs})$
Fetching the reactive component of $Z_{OFF}$ from Equ. 1 and equating to zero, the condition of resonance is obtained as:

$$R^2 = (X_L - Xcs)(X_{cg} - X_L + X_{cs}) \tag{2}$$

where, $X_L = \omega_r L, X_{cs} = 1/\omega_r C_s, \mathrm{X}_{cg} = 1/\omega_r C_g$

Obtaining the factors of Equ. 2, the resonant frequencies in the PIN OFF state are obtained as: $f_1 = 1/2\pi\sqrt{LC_s}, f_2 = \frac{1}{2\pi\sqrt{LC_s}}\sqrt{1 + \frac{C_g}{C_s}}$
Similarly, during the ON state, as the PIN diode acts as an RL circuit, the shunted gap capacitance, $C_g$ and the RL of diode behave as a parallel resonant circuit whose resonant frequency is $f_p =$

$1/2\pi\sqrt{L_sC_g}$. The impedance offered by this parallel resonant section (section 2.2) as shown in Fig. 4(b) is obtained as

$$Z_{ON} = [-jX_{cg} \times (R + jX_L)]/[-jX_{cg} + (R + jX_L)] \quad (3)$$

This variation in impedance caused by the switching states of the PIN diode results in shifts in resonant frequencies between lower and higher values. The optimized cell is simulated based on the infinite array approach and the magnitude and phase of the reflection coefficient is plotted against varying Malta cross size. The magnitude response curve in Fig. 5 shows dual resonance at 12 GHz and 9.5 GHz in the OFF condition of the PIN diode. A similar linear and smooth phase curve with 360° phase variation is obtained at both 12 GHz and 9.5 GHz.

**Table 1.** Parameters of the Proposed Unit cell

| **Parameter** | $E_s$ | $b$ | $w$,$L_s$,$dL$ | $W_P$ | $W_d$ | $h_1, h_2$ |
|---|---|---|---|---|---|---|
| Value(mm) | 12.5 | 8.5 | 0.3-1.6 | 2×(a/2-w-0.3) | 0.3 | 1.52 |

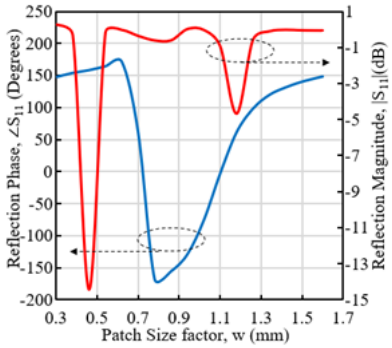


**Figure 5.** The reflection characteristics of the proposed unit cell

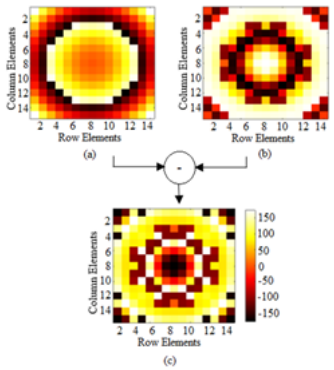


**Figure 6.** At 17 GHz (PIN ON state): (a) Required phase compensation matrix, (b) Simulated phase compensation matrix for varied w, (c) Phase error matrix to be compensated by varying dL

## 3. Reflectarray and ECB Design

A 225 element RRA ($18.75 \times 18.75cm^2$) is constructed on the Taconic substrate backed by metallic ground.

### 3.1. Frequency Reconfigurable RA

The reflection phase required for all 225 elements of the array is calculated at 12 GHz using MATLAB code based on the following equation (Carrasco et al., 2016):

Where $k_0$ is the free space propagation constant, $d_i$ is the distance between the centre of the ith element $(x_i, y_i)$ on the plane of reflectarray and the phase center of the feed and $(\theta_0, \varphi_0)$ is the main beam direction. When comparing these values with the unit cell phase curve in PIN OFF state, the size of the Malta cross in each unit cell is determined. In the PIN ON condition, the phase variation of the unit cell for varied Malta cross size is simulated and the phase error between the switching states of the diode is calculated. To compensate this phase error, phase curves of every element in the array at 17 GHz is simulated in PIN ON condition by varying the outer ring width, $dL$. When comparing the phase error matrix with these phase curves, the $dL$ value is determined for each array element. The phase error matrix computation for ON state operation of the PIN diode at 17 GHz is shown in Fig. 6.

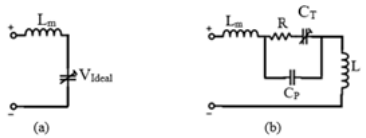


**Figure 7.** Equivalent circuit of varactor-based phase shifter for beam scanning: (a) Ideal and (b) Actual

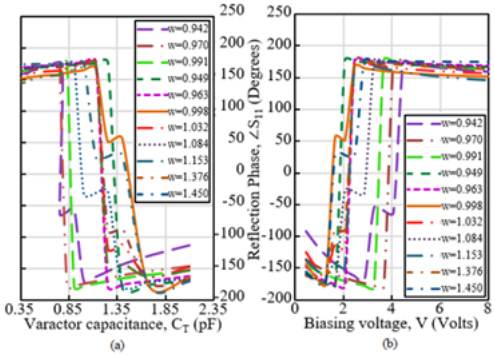


**Figure 8.** Reflection phase curves for fixed element sizes and varying (a) varactor capacitances and (b) varactor biasing voltages

### 3.2. Beam scanning

The designed frequency reconfigurable RA with varactor diodes in OFF condition offers the phase required for beam focussed in normal direction. To scan the obtained beam in different directions the phase compensation provided by each unit cell is changed in a controlled manner. This phase variation is obtained dynamically for every desired scanning angle by varying the capacitance of the corresponding varactor diode connected to the inductive element. The dimensions of the inductive element $(Lm)$ are selected based on the operating frequency and dielectric substrate. Skyworks SMV1231-079LF (Tian) is a silicon hyper-abrupt junction varactor used in this work for its low resistance and compatibility over 10 GHz. For initial full-wave simulations, the Varactor diode is modelled as an ideal varying capacitor $V_{Ideal}$ whose capacitance ranges from 2.35 pF to 0.466 pF for biasing voltage varied between 0 and 15 V. For array simulations, the actual equivalent parameters as shown in Table 2 are utilized. Figure 7 shows the series equivalent of the varactor and the inductive element with ideal and actual values. As the biasing voltage for the varactor diode continually varies, the RF choke connected between the stub and the biasing line acts as a DC block. In the ON and OFF state of PIN diode, for fixed sizes of the concentric structures, phase curves for various capacitance values of the varactor diode are obtained as shown in Fig. 8(a). The biasing voltages required for providing the respective capacitances are obtained from the datasheet of the varactor for every scanning angle. The difference between the phase required for generating beam in $\pm 10^{\circ}$ and the phase for normal direction beam is calculated. These

phase errors are compared with the phase curves obtained for varying varactor capacitances and the corresponding biasing voltage is provided to the varactors. Similarly, the biasing voltages of the varactors for steering beam to ±20° and ±30° are obtained.

### 3.3. Electronic Control Board

The dynamic control of beam scanning in the proposed compound reconfigurable RRA can be implemented using biasing voltages obtained from the ECB specifically designed for this purpose. The ECB includes three DAC60096 (Ti2, 2016) modules serially interfaced to a computer via an Arduino-based USB to SPI converter as shown in Fig. 9. The digital equivalent of the required biasing voltages for each scanning angle can be provided as input to the DAC units through a program developed using Arduino IDE software. The analog output of the DAC units is transferred to the biasing layer of the RRA through a 2328461 Standard Card Edge receptacle connector (Mou) having 280 pins.

**Table 2.** Equivalent Parameters of the Diodes

| Parameter (Unit) | PIN diode | | Varactor Diode |
|---|---|---|---|
| | OFF State | ON State | |
| Resistance, $R(\Omega)$ | 10 | 1 | 2.9 |
| Inductance, $L$(nH) | 0.7 | 0.7 | 0.7 |
| Capacitance, $C_T$(pF) | 0.21 | - | 0.466–2.35 (15 V–0 V) |
| Passive Capacitance, $C_p$(pF) | - | - | 0.44 |

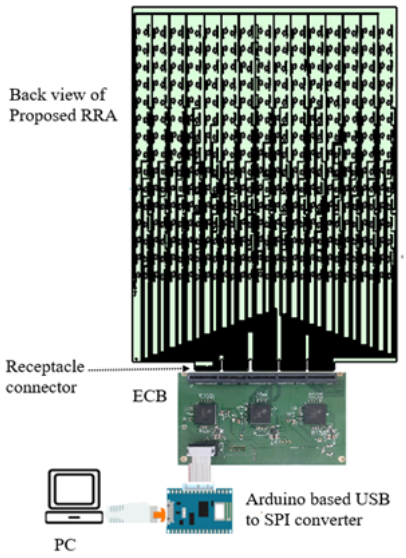


**Figure 9.** Integration between ECB and the proposed RRA

## 4. Analysis of RRA

The designed compound RRA is simulated in time domain under open space boundary conditions. The gap between the RRA and the source is maintained as 15 cm ($f/D = 0.8$) to obtain an optimal performance (Narayanasamy et al., 2021). The radiation pattern and gain at different frequencies within the operating ranges of the RRA in the two states of the PIN diode are observed. In each of these PIN diode states, the varactor diode biasing voltage is varied through the ECB and the changes in the radiation pattern are observed. The simulated patterns at different frequencies are plotted as in Fig. 10. In the OFF state of the PIN diode, the simulated side lobe levels are -14.8 dB at 12 GHz. At 9.5 GHz, the side lobe level is slightly more due to the presence of grating lobes. The simulated side lobe levels (SLL) at the PIN ON condition is observed as 13 dB at 17

GHz. Similarly, the cross-polarization levels in the ON and OFF state of the PIN diode are noted. At the PIN OFF state, a value less than -28 dB is observed at 12 GHz and 9.5 GHz, respectively.

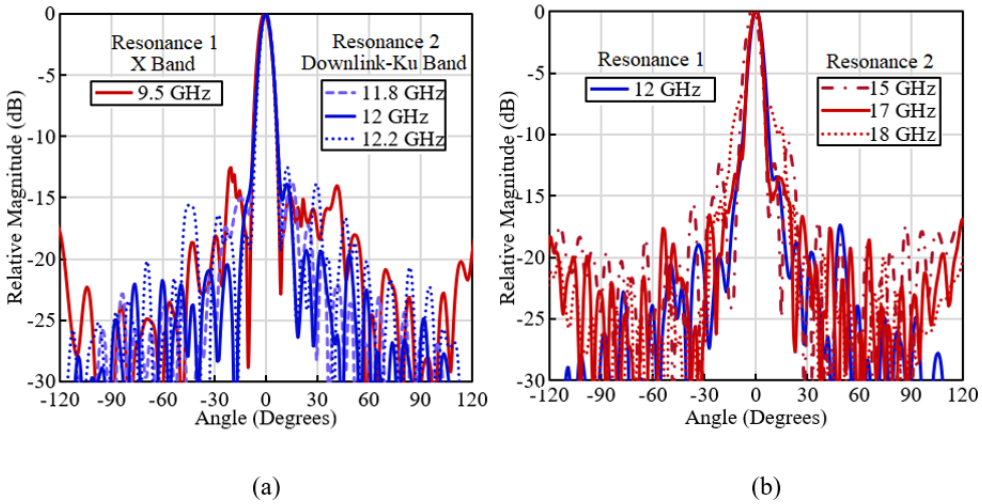


**Figure 10.** E-field radiation pattern for different frequencies at $\theta_{mb} = 0°$ in (a) PIN OFF condition and (b) PIN ON condition

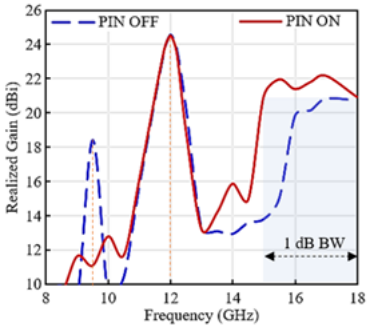


**Figure 11.** Gain vs frequency plot at $\theta_{mb} = 0°$ for varied states of PIN diode

The side lobe and cross-polarization levels at 9.5 GHz and 17 GHz are slightly higher than the values measured at 12 GHz due to the subwavelength size of the elements at lower range of frequency and occurrence of grating lobes at high frequency ranges. The required beam scanning angle $\theta_{mb}$ shall be fetched as input from the user using PC com port and communicated to the ECB through the USB to SPI converter as shown in Fig. 9. Based on the corresponding biasing voltages provided to each varactor by the DACs, the RRA integrated with the ECB shall produce beams scanned to $\pm 10$ ° and $\pm 20$ ° at 9.5 GHz. Owing to the increased complexities in attaining the set objectives, reduced degrees of freedom exist in the proposed design. A peak gain of 24.59 dBi and 18.43 dBi is obtained at 12 GHz and 9.5 GHz during the PIN OFF condition. The complete Ku-band downlink range of 11.8 to 12.2 GHz is covered in this state. In the PIN ON condition, same peak gain is maintained at 12 GHz and a peak gain of 22.16 dBi is obtained at 17 GHz. The 1 dB gain bandwidth observed at 17 GHz is 17.6% which covers 15 to 18 GHz range. Figure 11 depicts the simulated peak gain observed at different frequencies in the PIN OFF and PIN ON state.

## 5. Conclusion

A frequency agile $15 \times 15$ $(7.52 \times 7.52\lambda_0^2)$ reflectarray with beam steering capabilities is designed on 1.52-mm thick Taconic substrate backed by metallic ground. The compound reconfigurable RA

element has a Malta cross with diagonal slots of varying size enclosed within a square ring. The PIN diode connected between the concentric structures, switches the dual resonances among 12 GHz, 9.5 GHz, and 17 GHz, respectively. In the OFF state of the diode, a peak gain of 24.59 dBi and 18.43 dBi is obtained at 12 GHz and 9.5 GHz. In the PIN ON condition, a 22.16 dBi peak gain is obtained at 17 GHz while the resonance at 12 GHz remains the same. The SLL at 12 GHz, 9.5 GHz, and 17 GHz are observed as less than -14 dB and the cross-polarization level is observed as less than -30 dB, respectively. The controlled biasing of the varactors shall be implemented by integrating an ECB into the RRA through a receptale connector. Thus, the proposed compound RRA is the best suited in fixed satellite services and earth exploration satellites.

**Acknowledgement**

This work is supported by DST SERB under Core Research Grant (EMR/2017/001521)

**References**

Standard card edge receptacle connector datasheet. URL https://www.mouser.in/ProductDetail/TE-Connectivity/1-2328461-1.

Dac60096 96-channel, 12-bit, low-power, serial-input, high-voltage output dac with conversion trigger datasheet, 2016. URL https://www.ti.com/product/DAC60096.

Abbasi, M. I; Ismail, M. Y, and Kamarudin, M. R. Development of a pin diode-based beam-switching single-layer reflectarray antenna. *International Journal of Antennas and Propagation*, 2020, 2020. ISSN 16875877. doi: 10.1155/2020/8891759.

Boccia, L; Amendola, G, and Massa, G. D. Performance improvement for a varactor-loaded reflectarray element. *IEEE Transactions on Antennas and Propagation*, 58, 2010. ISSN 0018926X. doi: 10.1109/TAP.2009.2037697.

Carrasco, E; Barba, M, and Encinar, J. A. X-band reflectarray antenna with switching-beam using pin diodes and gathered elements. *IEEE Transactions on Antennas and Propagation*, 60, 2012. ISSN 0018926X. doi: 10.1109/TAP.2012.2208612.

Carrasco, E; Encinar, J. A, and Rahmat-Samii, Y. Reflectarray antennas: A review. In *Forum for Electromagnetic Research Methods and Application Technologies (FERMAT)*, volume 16, 2016.

Costanzo, S; Venneri, F; Massa, G. D; Borgia, A, and Raffo, A. Bandwidth performances of reconfigurable reflectarrays: State of art and future challenges. *Radioengineering*, 27, 2018. ISSN 12102512. doi: 10.13164/re.2018.0001.

Department of Telecommunications, G. O. I. National frequency allocation plan, 2018. URL https://dot.gov.in/spectrummanagement/committee-reviewrevision-national-frequency-allocation-plan-nfap-2018.

Gu, C; Gao, S; Sanz-Izquierdo, B; Parker, E. A; Li, W; Yang, X, and Cheng, Z. Frequency-agile beam-switchable antenna. *IEEE Transactions on Antennas and Propagation*, 65, 2017. ISSN 0018926X. doi: 10.1109/TAP.2017.2713978.

Hajian, M. Passive and active reconfigurable microstrip reflectarray antennas.

Han, J; Li, L; Liu, G; Wu, Z, and Shi, Y. A wideband 1 bit 12 × 12 reconfigurable beam-scanning reflectarray: Design, fabrication, and measurement. *IEEE Antennas and Wireless Propagation Letters*, 18, 2019. ISSN 15485757. doi: 10.1109/LAWP.2019.2914399.

Hum, S. V and Perruisseau-Carrier, J. Reconfigurable reflectarrays and array lenses for dynamic antenna beam control: A review. *IEEE Transactions on Antennas and Propagation*, 62, 2014. ISSN 0018926X. doi: 10.1109/TAP.2013.2287296.

Hum, S. V; Okoniewski, M, and Davies, R. J. Modeling and design of electronically tunable reflectarrays. *IEEE Transactions on Antennas and Propagation*, 55, 2007. ISSN 0018926X. doi: 10.1109/TAP.2007.902002.

Ismail, M; Inam, M, and Abdullah, J. Design optimization of reconfigurable reflectarray antenna based on phase agility technique. In *Third Conference on Antenna & RCS Measurement*. Citeseer, 2010.

Li, M; Wei, H; Zhao, J, and Tao, Q. Erratum: Trifrequency reconfigurable linear irregular array with beam deflection capability in x/ku/ka-bands(international journal of antennas and propagation (2020) 2020 (9074135) doi: 10.1155/2021/9074135). *International Journal of Antennas and Propagation*, 2021, 2021. ISSN 16875877. doi: 10.1155/2021/3805693.

Li, Y and Abbosh, A. Reconfigurable reflectarray antenna using single-layer radiator controlled by pin diodes. *IET Microwaves, Antennas and Propagation*, 9, 2015. ISSN 17518733. doi: 10.1049/iet-map.2014.0227.

Montori, S; Cacciamani, F; Gatti, R. V; Sorrentino, R; Arista, G; Tienda, C; Encinar, J. A, and Toso, G. A transportable reflectarray antenna for satellite ku-band emergency communications. *IEEE Transactions on Antennas and Propagation*, 63, 2015. ISSN 0018926X. doi: 10.1109/TAP.2015.2398128.

Narayanasamy, K; Mohammed, G. N. A; Savarimuthu, K; Sivasamy, R, and Kanagasabai, M. A comprehensive analysis on the state-of-the-art developments in reflectarray, transmitarray, and transmit-reflectarray antennas, 2020. ISSN 1099047X.

Narayanasamy, K; Mohammed, G. N. A; Savarimuthu, K; Sivasamy, R, and Kanagasabai, M. A novel ku/k band reflectarray antenna with reduced phase slope and phase sensitivity. *International Journal of RF and Microwave Computer-Aided Engineering*, 31, 2021. ISSN 1099047X. doi: 10.1002/mmce.22699.

Rodrigo, D; Jofre, L, and Perruisseau-Carrier, J. Unit cell for frequency-tunable beamscanning reflectarrays. *IEEE Transactions on Antennas and Propagation*, 61, 2013a. ISSN 0018926X. doi: 10.1109/TAP.2013.2281375.

Rodrigo, D; Jofre, L, and Perruisseau-Carrier, J. A frequency reconfigurable cell for beam-scanning reflectarrays. 2013b. doi: 10.1109/APS.2013.6711492.

Tayebi, A; Tang, J; Paladhi, P. R; Udpa, L; Udpa, S. S, and Rothwell, E. J. Dynamic beam shaping using a dual-band electronically tunable reflectarray antenna. *IEEE Transactions on Antennas and Propagation*, 63, 2015. ISSN 0018926X. doi: 10.1109/TAP.2015.2456939.

Tian, H. Electronically-tunable resonant blazed metasurface grating.

Trampler, M. E; Lovato, R. E, and Gong, X. Dual-resonance continuously beam-scanning x-band reflectarray antenna. *IEEE Transactions on Antennas and Propagation*, 68, 2020. ISSN 15582221. doi: 10.1109/TAP.2020.2989559.

Venneri, F; Costanzo, S, and Massa, G. D. Design and validation of a reconfigurable single varactor-tuned reflectarray. *IEEE Transactions on Antennas and Propagation*, 61, 2013. ISSN 0018926X. doi: 10.1109/TAP.2012.2226229.

Xu, H; Xu, S; Yang, F, and Li, M. Design and experiment of a dual-band 1 bit reconfigurable reflectarray antenna with independent large-angle beam scanning capability. *IEEE Antennas and Wireless Propagation Letters*, 19, 2020. ISSN 15485757. doi: 10.1109/LAWP.2020.3011578.

Yang, H; Yang, F; Xu, S; Mao, Y; Li, M; Cao, X, and Gao, J. A 1-bit 10 $\times$ 10 reconfigurable reflectarray antenna: Design, optimization, and experiment. *IEEE Transactions on Antennas and Propagation*, 64, 2016. ISSN 0018926X. doi: 10.1109/TAP.2016.2550178.

Yang, H; Yang, F; Cao, X; Xu, S; Gao, J; Chen, X; Li, M, and Li, T. A 1600-element dual-frequency electronically reconfigurable reflectarray at x/ku-band. *IEEE Transactions on Antennas and Propagation*, 65, 2017. ISSN 0018926X. doi: 10.1109/TAP.2017.2694703.

Zhang, H; Chen, X; Wang, Z; Ge, Y, and Pu, J. A 1-bit electronically reconfigurable reflectarray antenna in x band. *IEEE Access*, 7, 2019. ISSN 21693536. doi: 10.1109/ACCESS.2019.2918231.